Heliyon 10 (2024) e34199

Contents lists available at ScienceDirect

Heliyon

journal homepage: www.cell.com/heliyon

Research article

Rapid degradation of perfluorooctane sulfonic acid (PFOS) and perfluorononanoic acid (PFNA) through bimetallic catalyst of Fe_2O_3/Mn_2O_3 and unravelling the effect of support SiO_2

Junyoung Park [a,b], Jong Kwon Choe [a,b], Jiyeol Bae [c], Soyoung Baek [c,*]

[a] Department of Civil and Environmental Engineering, Seoul National University, Seoul, 08826, South Korea
[b] Institute of Construction and Environmental Engineering, Seoul National University, Seoul, 08826, South Korea
[c] Department of Environment Research, Korea Institute of Civil Engineering and Building Technology (KICT), Goyang, 10223, South Korea

ARTICLE INFO

Keywords:
PFAS
Catalytic oxidation
Fenton reaction
Photocatlysis

ABSTRACT

Perfluoroalkyl substances (PFAS) are emerging contaminants present in various water sources. Their bioaccumulation and potential toxicity necessitate proper treatment to ensure safe water quality. Although iron-based monometallic photocatalysts have been reported to exhibit rapid and efficient PFAS degradation, the impact of bimetallic photocatalysts is unknown. In addition, the mechanistic effects of utilizing a support are poorly understood and solely based on physicochemical properties. This study investigates the efficacy of bimetallic photocatalysts (Fe_2O_3/Mn_2O_3) in inducing the photo-Fenton reaction for the degradation of perfluorooctane sulfonate (PFOS) and perfluorononanoic acid (PFNA) under various conditions. The rapid removal of both PFAS was observed within 10 min, with a maximum efficiency exceeding 97 % for PFOS under UV exposure, aided by the photocatalytic activation (photo-Fenton) of the oxidant (H_2O_2). Contrary to expectations, the use of the SiO_2 support material did not significantly improve the removal efficiency. The efficacy of PFNA decreased despite SiO_2 providing larger surface areas for Fe_2O_3/Mn_2O_3 loading. Further analysis revealed that the adsorption of PFAS onto the catalyst surfaces owing to electrostatic interactions contributed to the removal efficiency, where the degradation efficacy was worse than that of the catalyst with SiO_2. This is because adsorption hindered the effective contact of H_2O_2 with catalytic reaction sites, thereby impeding the generation of hydroxyl (·OH) radicals. This study indicates the importance of considering chemical properties, including surface charge, in catalyst design to ensure effective degradation, focusing on physicochemical properties, such as surface area might overlook crucial factors.

1. Introduction

Per- and polyfluoroalkyl substances (PFAS) raise emerging concerns because of their ubiquitous presence in environmental media, especially in drinking water, and their potential toxic profiles upon consistent ingestion of water contaminated with PFAS [1]. Considering the structure of PFAS, fluorine atoms are fully or partially attached to the carbon skeleton, which make them as “forever chemicals” owing to the high persistency that are hardly degraded in nature [2]. In addition, owing to their fluorinated carbon structure, PFAS easily accumulate in the human body, causing potential chronic toxicity, including carcinogenicity [3]. Several animal

* Corresponding author.
E-mail address: soyoung@kict.re.kr (S. Baek).

https://doi.org/10.1016/j.heliyon.2024.e34199
Received 4 May 2024; Received in revised form 11 June 2024; Accepted 4 July 2024
Available online 5 July 2024

studies have investigated the liver toxicity of PFAS, which have been reported to act as hormone disruptors that alter lipid metabolism, yield higher levels of cholesterol, and eventually cause hepatic steatosis [4,5]. Therefore, it is necessary to develop appropriate treatment systems, monitoring techniques, and toxicity assessments to ensure water quality [6].

Several attempts have been made to degrade PFAS in water via photocatalysis, sonolysis, thermal degradation, and electrochemical oxidation [7,8]. However, despite their high efficiency, the reported studies are usually time-consuming, along with the high cost of operation (i.e., the use of large amounts of energy) [9]. Alternatively, biodegradation seems promising in terms of cost-effectiveness and eco-friendliness compared with physical and chemical processes. However, biodegradation requires an ample amount of time; Park et al. found that the degradation of perfluorooctanoic acid requires more than 40 days to achieve ~60–80 % removal efficiency [10].

Thus, Fe-based catalysts can overcome these drawbacks. Its oxide form of iron catalysts can generate powerful reactive oxygen species (ROS), such as hydroxyl (·OH) radical [11]. Schlesinger et al. successfully synthesized Fe_3O_4 catalysts to induce a Fenton-like reaction and degraded 90 % of the maximum within 30 min with the aid of UV [12]. Because iron-based catalyst has characteristic of semiconductor, the electron is separated from the valence band (yielding a positive hole) upon a UV irradiation to facilitate hydroxyl (·OH) radical generation in addition to Fenton-like reaction. Therefore, an iron-based photocatalyst is an effective chemical treatment for PFAS degradation. However, we were intrigued if bimetallic catalyst could further enhance the degradation efficacy, because bimetallic catalysts have been reported to enhance the catalytic performances compared to the monometallic catalysts owing to advantage of the metal dispersion and increase in active site [13,14]. In addition, catalysts, such as Mn_2O_3, induce Fenton-like reactions that generate hydroxyl (·OH) radicals [15]. It is assumed that the Mn-assisted Fe-based bimetallic catalyst synergistically improves catalytic performance. Furthermore, mesoporous support materials (i.e., SiO_2) are known to enhance the dispersivity of metallic catalysts, such that SiO_2 provides large surface areas and can pack metallic catalysts with a high density for better catalytic reactions [16]. However, the mechanism behind the use of support materials is poorly understood as to whether the support always facilitates catalytic degradation owing to its physicochemical properties.

Here, we show the degradation of two PFAS, perfluorooctane sulfonic acid (PFOS) and perfluorononanoic acid (PFNA), which differ only in their functional groups (carboxyl and sulfonyl groups, respectively). Specifically, bimetallic catalysts of Fe_2O_3/Mn_2O_3 were synthesized to investigate the degradation of PFAS under various conditions (i.e., H_2O_2 and H_2O_2 + UV). Subsequently, the impact of the support (SiO_2) was assessed to elucidate the effect of the support materials on adsorption. Finally, we provide a mechanistic explanation that may offer insights into the consideration of more important features than physicochemical properties for the better design and proper usage of support materials.

2. Materials and methods

2.1. Chemicals

Manganese (II) nitrate tetrahydrate ($Mn(NO_3)_2{\cdot}4H_2O$, >98 %), ferric (III) nitrate nonahydrate ($Fe(NO_3)_3{\cdot}9H_2O$), and cetyltrimethylammonium chloride (CTAC) solution (25 wt %) were purchased from Sigma Aldrich, Germany. Hydrogen peroxide (28 % H_2O_2) solution and sodium hydroxide (1 N NaOH) were supplied by Daejung Chemicals and Metals Co., Ltd., Korea. Tetraethyl Orthosilicate 95 % (TEOS) was purchased from Samchun Company (South Korea). Perfluorooctanesulfonic acid (PFOS) and Perfluorononanoic acid (PFNA) were purchased from Sigma–Aldrich.

2.2. Synthesis of bimetallic catalyst

Fe_2O_3/Mn_2O_3 was synthesized using a coprecipitation method. Fe(NO3)3·9H2O and Mn(NO3)2·4H2O were dissolved in DI water and warmed up to 65 °C for 30 min. Subsequently, Cetyltrimethylammonium chloride (CTAC) was mixed with the solution for 120 min at 65 °C. NaOH solution was introduced as a precipitation agent while applying sonication until reaching a pH of 12. The precipitated sample underwent washing with DI water, followed by dehydration at 100 °C for 24 h, and finally, calcination at 700 °C for 7 h.

Fe_2O_3/Mn_2O_3@SiO_2 was synthesized using the following procedure. Initially, Fe_2O_3/Mn_2O_3nanoparticles were mixed with CTAC for 30 min at 40 °C. Subsequently, TEOS was introduced into the mixture, resulting in the immediate formation of a black gel. This gel was then incubated for 24 h at 50 °C under a 200 rpm stirrer. Following incubation, the gel was calcined in a furnace and ramped at a rate of 2 °C/min until it reached 550 °C, which was maintained for 6 h.

2.3. Characterization

Images of the developed catalysts were obtained using scanning electron microscopy (SEM) with a Hitachi S-4800 instrument (Japan). Elemental mapping in two dimensions (2D) was conducted using energy-dispersive X-ray spectroscopy (EDS) using an X-Maxn 80 T instrument (Oxford, UK). Transmission electron microscope (TEM) images were acquired using a Philips CM200 instrument. A Gemini series Micromeritics 2360 instrument was used for the Brunauer-Emmett-Teller (BET) analysis. Fourier transform infrared (FTIR) spectra of the samples were recorded using a PerkinElmer FTIR spectrometer. For X-ray photoelectron spectroscopic (XPS) analysis, a Kratos Axis Ultra XPS instrument was utilized.

2.4. Degradation experiment

PFOS and PFNA were selected as the target pollutants to evaluate the efficacy of the developed bimetallic catalysts under various oxidation and adsorption conditions. A 200 mL solution containing the target pollutants at a concentration of 2 mg L−1 was prepared. Subsequently, 25 mmol L−1 of 28 % H_2O_2 was introduced into the solution, followed by an addition of 100 mg of the catalysts. No pH adjustments were made, and the initial pH of the solution was 7.3.

The experiments were conducted in a black acrylic reactor with a quartz tube and four UV lamps around the quartz tube. The reactor temperature was maintained at 25 °C using cooling fans, and UV-C lamps (8 W, λ max = 254 nm, Philips) served as the irradiation source for the experiments. The degradation of PFOS and PFNA solutions was monitored under varying UV light exposure conditions. Samples were collected at 0, 5, 10, and 20 min. The samples were analyzed using liquid chromatography-tandem mass spectrometry (LC/MS/MS) on a Thermo Vanquish system (Thermo Scientific, Waltham, MA, USA) equipped with a tandem mass spectrometer (TSQ Quantis, Thermo Fisher Scientific, USA). For chromatographic separation, Waters Cortects C18 (2.1 × 100, 1.6 μm) column was used and maintained at 45 °C, and the flow rate was set to 0.3 mL/min. The sample injection volume was 10 μL, and the gradient was formed by changing the mixing ratio of solvent A (1 mM NH_4F in deionized water) and solvent B (0.1 % formic acid in methanol). Analyses were performed with experimental triplicates to ensure accuracy and reproducibility. Analyses were performed with experimental triplicate to ensure accuracy and reproducibility.

3. Results and discussion

3.1. Catalyst characterization

Prior to investigating the degradation efficiency, the physicochemical properties were assessed to validate whether the two catalysts were properly synthesized with a homogeneous distribution of metals. SEM analysis was performed to investigate the morphology and structure of the synthesized Fe_2O_3/Mn_2O_3; the results are shown in Fig. 1a. The SEM image shows a porous coral-like architecture of Fe_2O_3/Mn_2O_3, which can be attributed to the role of the CTAC surfactant in the synthesis. The 2D-mapping of Fe_2O_3/Mn_2O_3 confirmed the presence of constituent elements on the surface of the synthesized photocatalyst, and no other elemental impurities were detected. Moreover, the constituent elements Fe, Mn, and O were homogeneously dispersed in the photocatalyst (Fig. 1b–e). Note that the presence of oxygen at a high density may be owing to the adsorbed water molecules.

To characterize the microstructure and elemental composition, high-resolution TEM (HRTEM) and EDS analyses were conducted. The nanoparticles (NPs) showed a hexagonal morphology with overlapping particles (Fig. 2a). TEM-EDS mapping confirmed the distribution of Fe_2O_3 and Mn_2O_3 NPs over the entire region (Fig. 2b–e). The 2D map of 'Mn' significantly overlapped with that of the 'Fe,' suggesting a close proximity of Mn_2O_3 NPs with the Fe_2O_3 NPs.

XPS analysis was performed to study the composition and oxidation states of the elements in the Fe_2O_3/Mn_2O_3 photocatalyst (Fig. 3a). The XPS survey spectrum of the Fe_2O_3/Mn_2O_3 photocatalyst confirms the presence of Fe, Mn, and O in the sample, and the observed carbon peak is attributed to the CTAC surfactant used in the synthesis. The O 1s HRXPS spectrum in Fig. 3b shows two intense peaks at 529.80 and 530.95 eV, which are attributed to the metal-oxygen bonds (lattice oxygen) and oxygen defect sites, respectively [17]. Fig. 3c shows the HRXPS Fe 2p spectrum, with two dominant peaks at 710.64 and 724.14 eV, which were assigned to Fe 2P3/2 and Fe 2P1/2, respectively. Moreover, the presence of satellite peaks at 719.01 and 732.15 eV further confirmed the existence of Fe_2O_3 species [18–20]. Fig. 3d shows the Mn 2p high-resolution XPS spectrum, where the two peaks can be attributed to Mn 2p3/2 (641.80 eV) and Mn 2p1/2 (652.92 eV) [21] with a typical splitting energy of ~12 eV, suggesting the presence of Mn^{3+}, which corresponds to Mn_2O_3 species [22].

Similarly, Fe_2O_3/Mn_2O_3 @SiO_2 was successfully synthesized, in which the Fe and Mn atoms were well distributed on the surface of the spherical nanoparticles of the SiO_2 support (Fig. 4). Furthermore, the elemental spectrum and 2D-mapping of the synthesized

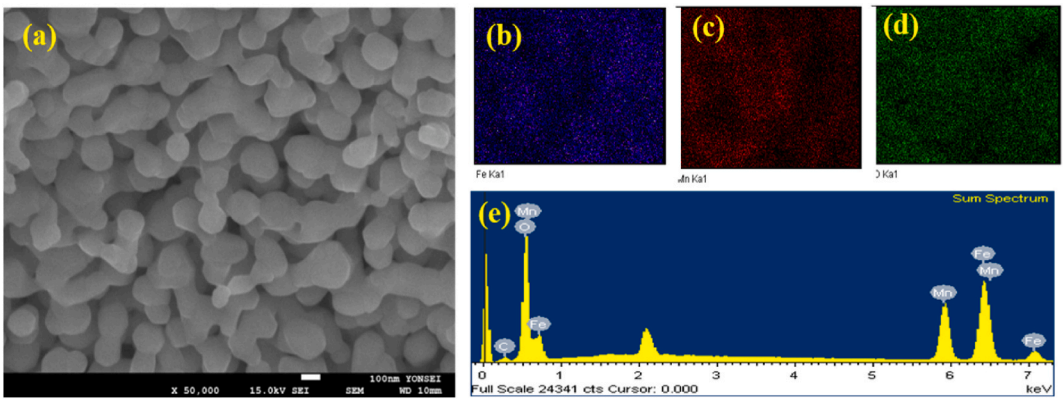

Fig. 1. (a) SEM micrograph (b) EDS spectrum (c) O 2D map (d) Fe 2D map (e) Mn 2D map of Fe_2O_3/Mn_2O_3 photocatalyst.

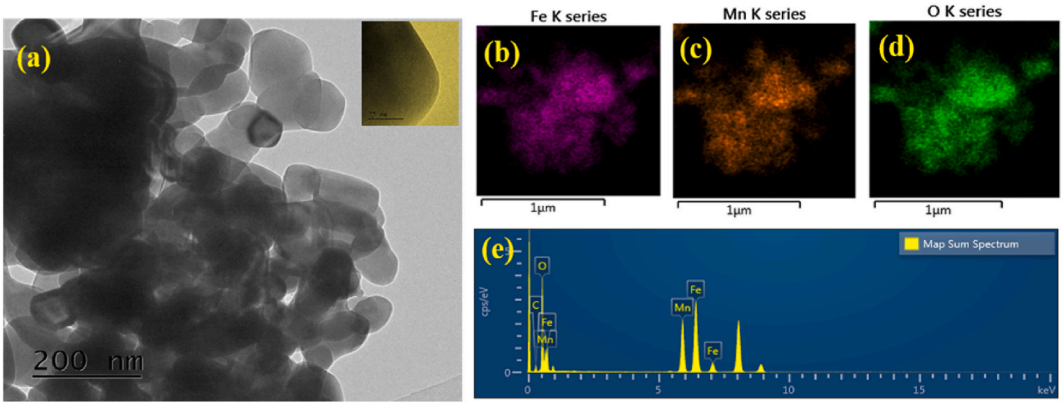

Fig. 2. (a) TEM micrograph (b) EDS mapping (c) Mn 2D map (d) Fe 2D map (e) O 2D map of Fe_2O_3/Mn_2O_3 photocatalyst.

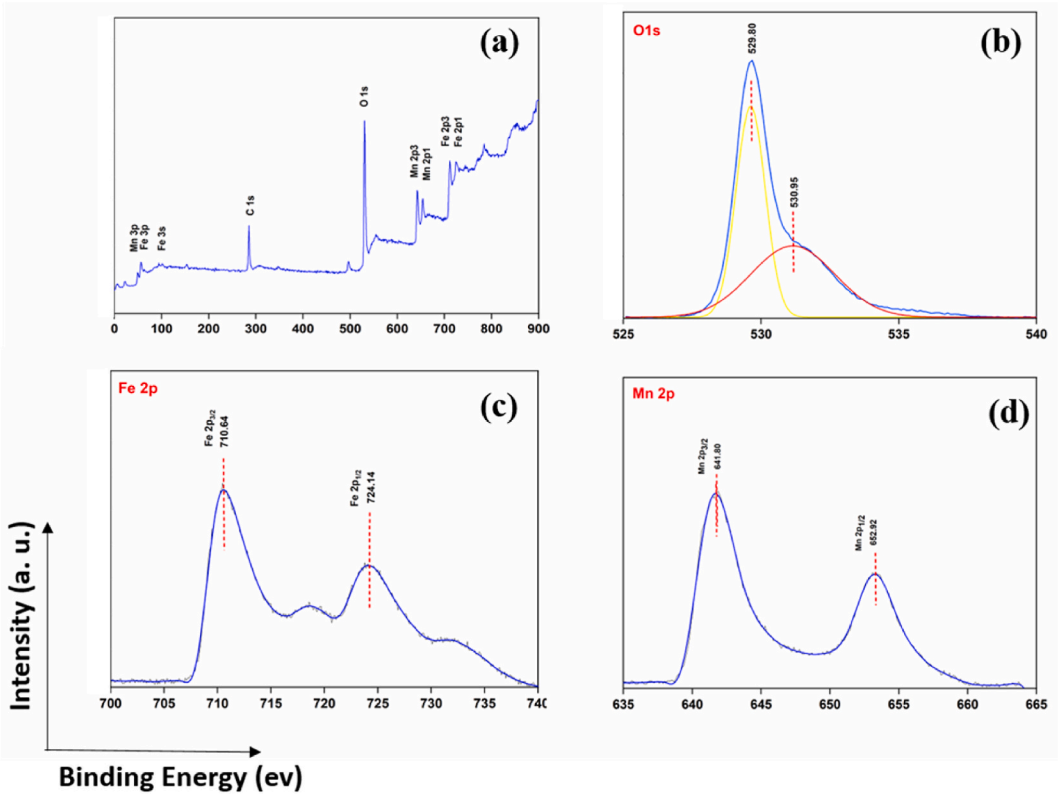

Fig. 3. (a) XPS scan survey; (b) HRXPS O 1s; (c) HRXPS Mn 2p; (d) HRXPS Fe 2p spectra of Fe_2O_3/Mn_2O_3 photocatalyst.

catalysts contained the intended metal components with high purity, and non-specific species were undetected.

3.2. Removal efficiency of PFNA and PFOS via catalysts

Catalytic oxidation of PFNA and PFOS was observed under various conditions to induce the Fenton reaction using H_2O_2. As shown in Fig. 5, H_2O_2, UV, and H_2O_2 + UV do not significantly influence the degradation of PFOS and PFNA without the addition of a catalyst. Although in the case of PFOS, H_2O_2 showed the potential for degradation, where H_2O_2 itself presumably could degrade PFOS, the degradation effect was minimal, indicating that the oxidation potential was insufficient. Overall, the result suggested H_2O_2 activation owing to the Fenton reaction by iron-based catalysts significantly affecting the degradation of both compounds where the production of stronger oxidant of hydroxyl (·OH) radicals are important and key parameters to effectively degrade PFAS compounds [23]. In addition, the removal efficacy of the photocatalysts (Fe_2O_3/Mn_2O_3 with/without a SiO_2 support) was further improved by UV

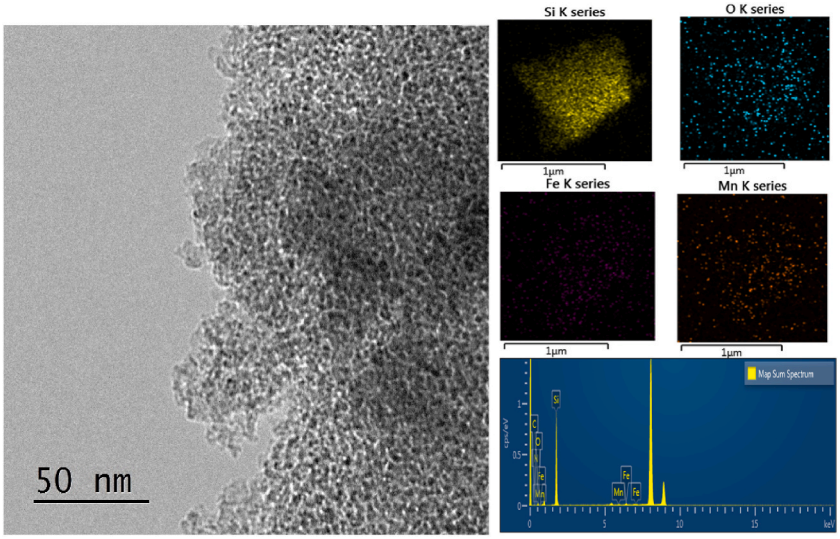

Fig. 4. TEM micrograph and EDS mapping Si, O, Fe, Mn of Fe_2O_3/Mn_2O_3 @ SiO_2.

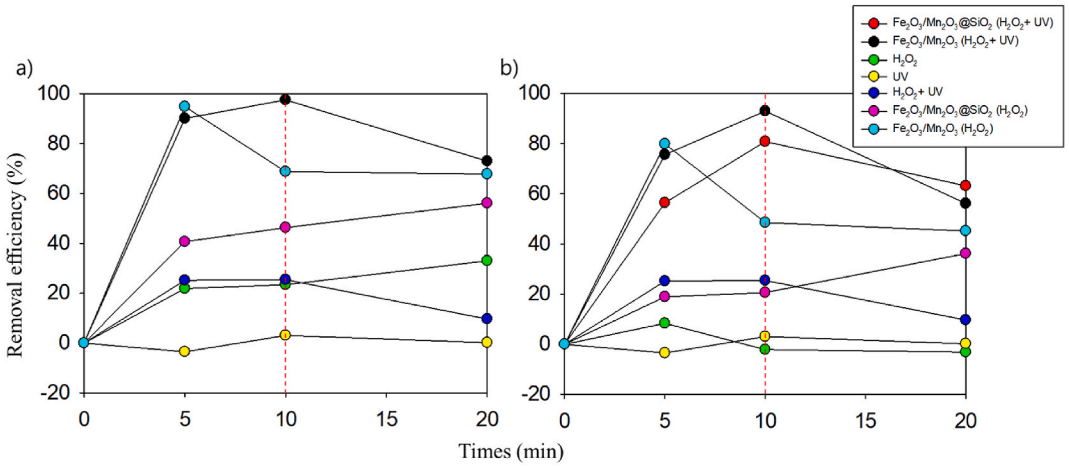

Fig. 5. Removal efficiency of a) PFOS and b) PFNA in various conditions. The red dashed bar indicates the reaction time at which maximum removal efficiency was achieved. In case of PFOS, the curves of Fe_2O_3/Mn_2O_3 with/without SiO_2 (H_2O_2 + UV) is overlapped. (For interpretation of the references to colour in this figure legend, the reader is referred to the Web version of this article.)

exposure, followed by the removal of >97 % of PFOS and 80–93 % of PFNA in the first 10 min of the reaction. This is attributed to the foster of hydroxyl (·OH) radical generation owing to the photocatalytic activation where the electron and positive holes are separated between conduction and valence bands to either oxidize OH^- or reduce H_2O_2 to yield hydroxyl (·OH) radical under the UV system. Overall, achieving a removal efficiency of over 97 % for PFOS within 10 min indicates rapid and effective degradation, whereas Schlesinger et al. [12] achieved nearly 90 % PFOS degradation over a longer period (30 min) using a monometallic photocatalyst of Fe_3O_4. This highlights the synergistic benefits of the bimetallic catalysts, which outperform the monometallic catalysts used in a previous study in terms of both removal efficiency and rapidity. Both metal species in Fe_2O_3 and Mn_2O_3 demonstrate the ability to activate H_2O_2, generating hydroxyl (·OH) radicals through a Fenton-like reaction, in addition to their photocatalytic activation as depicted in equations (1)–(5) [24].

$$Fe^{3+}\ (\text{or } Mn^{3+}) + H_2O_2 \rightarrow Fe^{2+}\ (\text{or } Mn^{2+}) + \cdot OOH + H^+ \quad (1)$$

$$Fe^{2+}\ (\text{or } Mn^{2+}) + H_2O_2 \rightarrow Fe^{3+}\ (\text{or } Mn^{3+}) + \cdot OH + OH^- \quad (2)$$

$$Fe_2O_3/Mn_2O_3 + h\nu \rightarrow e^- + h^+ \quad (3)$$

$$e^- + H_2O_2 \rightarrow \cdot OH + OH^- \quad (4)$$

$$h^+ + OH^- \rightarrow \cdot OH \quad (5)$$

However, the removal efficiency of Fe_2O_3/Mn_2O_3 was either similar (for PFOS) or even higher (for PFNA) in the first 10 min. BET analysis of N_2 adsorption-desorption (Fig. 6) indicated surface area of 14.67 m^2/g and 926 m^2/g for Fe_2O_3/Mn_2O_3 and Fe_2O_3/Mn_2O_3 @SiO_2, respectively. We originally assumed that loading metal catalysts onto a support metal, such as SiO_2 would be efficient, as the surface area of the catalytic metals would be larger to provide broader reaction sites and H_2O_2 binding sites for ease of activation. Furthermore, Fe_2O_3/Mn_2O_3 @SiO_2 exhibited typical mesopores (type IV), whereas the metallic catalysts did not contain any pores in terms of morphology (Fig. 6a–b). Altogether, the results of the TEM and BET analyses suggest that SiO_2 provides large surface areas with mesoporous structures, where Fe_2O_3 and Mn_2O_3 are densely packed within the pores for better catalytic reactions. Other parameters should be considered for a better understanding of the degradation efficacy. Therefore, we were intrigued to further investigate the disparity between the efficacy and surface area.

3.3. Effect of support materials and adsorption

Several studies have reported the adsorption capacity of either iron or manganese oxide for target compounds took in place; thus, contributing to the overall removal efficiency [25–28]. Nevertheless, the use of metallic catalysts (in the context of the Fenton reaction) aims to "degrade" the compounds rather than simply "remove" them for efficient mineralization. This distinction is crucial because focusing solely on removal may underestimate the true efficacy of the catalytic performance. Therefore, it is essential to assess the catalytic reaction that accounts for the contribution of removal owing to the actual degradation of the target compounds. Careful examination of the incubation of PFAS and the catalysts over 20 min showed that the adsorption capacities of PFOS (within 10 min) and PFNA (within 20 min) were higher in Fe_2O_3/Mn_2O_3 than in Fe_2O_3/Mn_2O_3 @SiO_2 (Fig. 7). In particular, the adsorption of PFNA deviated significantly, reaching 80-fold after 10 min of incubation with the catalyst on the support SiO_2 was applied.

The adsorption capacity could be attributed to the surface charges of the catalysts and the negative charges on the functional groups of PFAS. First, the zeta potential of SiO_2 was negative at a pH of 7.3. The FTIR study (Fig. 8a) shows an increase in the number of hydroxyl groups (peak at 3460 cm^{-1}) with Si–*O*–Si bonds at 1100 cm^{-1} in the case of Fe_2O_3/Mn_2O_3 @SiO_2 [29]. The SiO_2 support altered the surface charges, contributing to negative charges owing to the deprotonated hydroxyl functional groups in the aqueous state. XPS analysis further confirmed the formation of hydroxyl functional groups on SiO_2 at 533.23 eV (atomic % of 31.85) in the O 1s spectrum (Fig. 8b) [30]. Secondly, the PFOS and PFNA species are usually anionic, with pKa values near zero, and the functional head groups should possess a negative partial charge. This refers to the degree of electrostatic attraction and repulsion between the negative charges on the PFAS and the relatively positive (Fe_2O_3/Mn_2O_3) or negative (Fe_2O_3/Mn_2O_3 @SiO_2) surface charges of the catalysts. PFNA has a higher solubility, leading to a higher portion of the anionic state in the solution; thus, electrostatic repulsion is relatively emphasized, explaining why PFNA is poorly adsorbed on Fe_2O_3/Mn_2O_3 @SiO_2.

Therefore, it is important to understand whether good adsorption results in better PFAS degradation efficacy. To validate the removal efficiency, normalization was performed to investigate the contribution of degradation owing to hydroxyl radicals by subtracting the adsorbed concentration from the total removed levels (Fig. 9). However, the degradation of PFAS was negatively correlated with adsorption, and the efficiency of PFOS and PFNA degradation worsened when the adsorbed levels increased. We speculated PFAS adsorbed into the surface of the catalysts causing surface blockage where oxidants of H_2O_2 could not transform into the hydroxyl (·OH) radical as shown in proposed mechanism of Fig. 10. These results suggest that adsorption may hinder degradation owing to surface blockage by hindering the Fenton reaction to ease the destruction of PFAS. Therefore, it is crucial to consider chemical properties, including surface charges when designing catalysts to achieve effective degradation, rather than focusing solely on physicochemical properties, such as surface area. This is because our study indicated that adsorption could potentially hinder degradation.

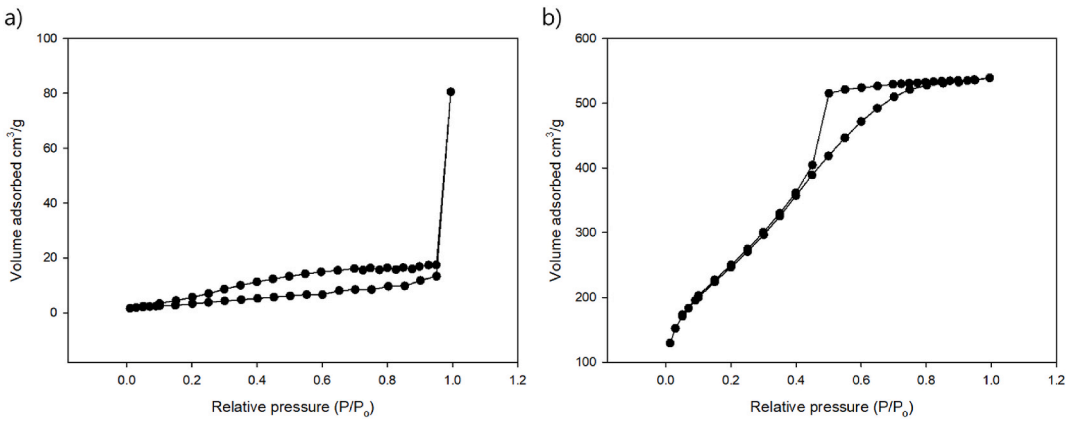

Fig. 6. N_2 adsorption-desorption isotherm curve and pore size distribution of a) Fe_2O_3/Mn_2O_3 and b) Fe_2O_3/Mn_2O_3 @SiO_2.

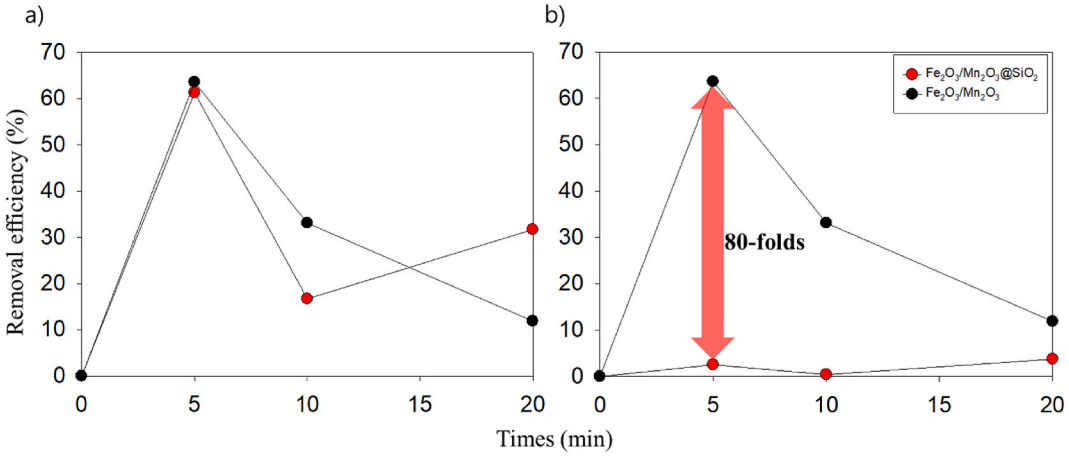

Fig. 7. Removal efficiency of a) PFOS and b) PFNA by adsorption.

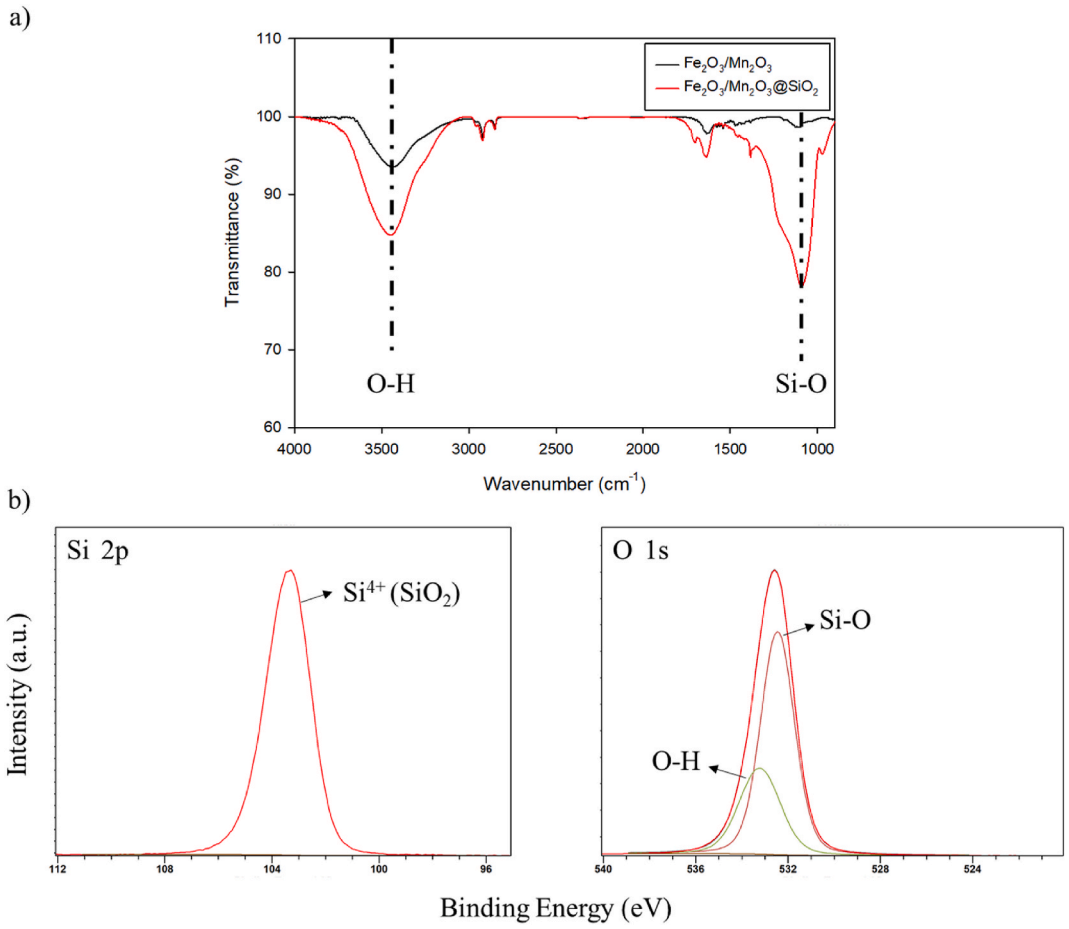

Fig. 8. a) FTIR analysis of photocatlaysts and b) HRXPS Si 2p and O 1s spectra of Fe_2O_3/Mn_2O_3 @SiO_2.

4. Conclusion

This study investigated the impact of bimetallic photocatalysts on the photodegradation of PFOS and PFNA under various conditions. The removal of both PFAS occurred rapidly in 10 min, with a maximum efficiency >97 % for PFOS under UV exposure, with the aid of photocatalytic activation (photo-Fenton) of the oxidant (H_2O_2) in addition to the Fenton reaction. In particular, we found

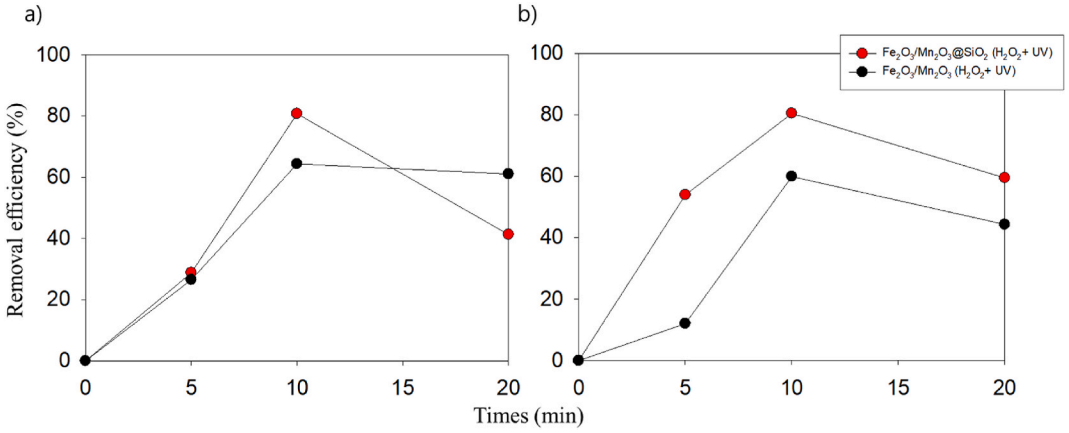

Fig. 9. Degradation effect of a) PFOS and b) PFNA solely due to the Fenton reaction activated by UV.

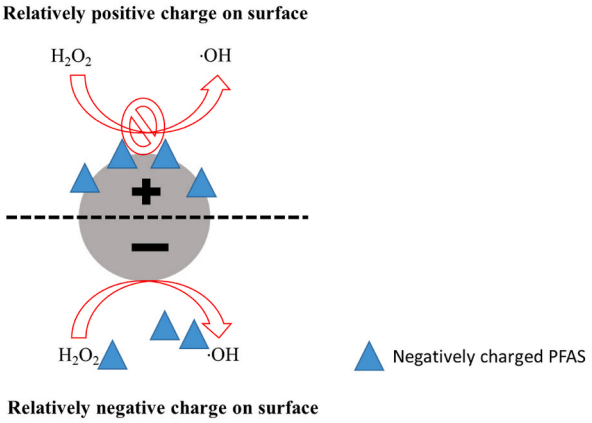

Fig. 10. Proposed mechanism of adsorption impact on catalytic activation of H_2O_2.

that the bimetallic (Fe_2O_3/Mn_2O_3) catalysts synergistically interacted with each other to enhance the removal efficiency compared with the monometallic catalyst of Fe_2O_3 reported in a previous study [12]. Furthermore, the utilization of support material of SiO_2 does not significantly improve the removal efficiency, whereas in the case of PFNA, the efficacy was worse, although SiO_2 provided larger surface areas for Fe_2O_3/Mn_2O_3 loading. However, when normalization was conducted solely to assess the degradation efficacy by excluding the adsorption amount, the degradation efficacy of Fe_2O_3/Mn_2O_3 was relatively poor compared to that of the catalysts with support materials. This was attributed to the adsorption of PFAS onto the catalyst surface owing to electrostatic interactions, which hindered H_2O_2 from effectively contacting the catalytic sites and adversely affected the generation of hydroxyl (·OH) radicals, suggesting the importance of chemical properties (i.e., surface charges), when designing catalysts to ensure effective degradation. The current research aims to identify the byproducts to determine if the reaction pathways are consistent for both Fe_2O_3/Mn_2O_3 and $Fe_2O_3/Mn_2O_3@SiO_2$, helping to confirm whether adsorption solely decreases the production of ·OH radicals. This study provides insights into the mechanistic impact of support materials, contributing to the better design of photocatalysts.

Funding statement

This research was supported by the Korean Ministry of Environment, as part of the Aquatic Ecosystem Conservation Research Program (No. 20240214–001).

Data availability statement

Data will be made available on request.

Additional information

No additional information is available for this paper.

CRediT authorship contribution statement

Junyoung Park: Writing – original draft, Visualization, Methodology, Investigation, Conceptualization. **Jong Kwon Choe:** Writing – review & editing. **Jiyeol Bae:** Writing – review & editing. **Soyoung Baek:** Writing – review & editing, Supervision, Resources, Methodology, Funding acquisition, Conceptualization.

Declaration of competing interest

The authors declare that they have no competing financial interests or personal relationships that may have influenced the work reported in this study.

References

[1] E.M. Sunderland, X.C. Hu, C. Dassuncao, A.K. Tokranov, C.C. Wagner, J.G. Allen, A review of the pathways of human exposure to poly- and perfluoroalkyl substances (PFASs) and present understanding of health effects, J. Expo. Sci. Environ. Epidemiol. 29 (2019) 131–147, https://doi.org/10.1038/s41370-018-0094-1.

[2] H. Brunn, G. Arnold, W. Körner, G. Rippen, K.G. Steinhäuser, I. Valentin, PFAS: forever chemicals—persistent, bioaccumulative and mobile. Reviewing the status and the need for their phase out and remediation of contaminated sites, Environ. Sci. Eur. 35 (2023) 20, https://doi.org/10.1186/s12302-023-00721-8.

[3] K. Steenland, A. Winquist, PFAS and cancer, a scoping review of the epidemiologic evidence, Environ. Res. 194 (2021) 110690, https://doi.org/10.1016/j.envres.2020.110690.

[4] R. Jin, R. McConnell, C. Catherine, S. Xu, D.I. Walker, N. Stratakis, D.P. Jones, G.W. Miller, C. Peng, D.V. Conti, M.B. Vos, L. Chatzi, Perfluoroalkyl substances and severity of nonalcoholic fatty liver in Children: an untargeted metabolomics approach, Environ. Int. 134 (2020) 105220, https://doi.org/10.1016/j.envint.2019.105220.

[5] M. Haug, L. Dunder, P.M. Lind, L. Lind, S. Salihovic, Associations of perfluoroalkyl substances (PFAS) with lipid and lipoprotein profiles, J. Expo. Sci. Environ. Epidemiol. 33 (2023) 757–765, https://doi.org/10.1038/s41370-023-00545-x.

[6] J. Park, K.-A. Yang, Y. Choi, J.K. Choe, Novel ssDNA aptamer-based fluorescence sensor for perfluorooctanoic acid detection in water, Environ. Int. 158 (2022) 107000, https://doi.org/10.1016/j.envint.2021.107000.

[7] J.N. Meegoda, B. Bezerra De Souza, M.M. Casarini, J.A. Kewalramani, A review of PFAS destruction technologies, IJERPH 19 (2022) 16397, https://doi.org/10.3390/ijerph192416397.

[8] R.K. Singh, S. Fernando, S.F. Baygi, N. Multari, S.M. Thagard, T.M. Holsen, Breakdown products from perfluorinated alkyl substances (PFAS) degradation in a plasma-based water treatment process, Environ. Sci. Technol. 53 (2019) 2731–2738, https://doi.org/10.1021/acs.est.8b07031.

[9] A. Berhanu, I. Mutanda, J. Taolin, M.A. Qaria, B. Yang, D. Zhu, A review of microbial degradation of per- and polyfluoroalkyl substances (PFAS): biotransformation routes and enzymes, Sci. Total Environ. 859 (2023) 160010, https://doi.org/10.1016/j.scitotenv.2022.160010.

[10] J. Park, S. Huang, B.E. Koel, P.R. Jaffé, Enhanced Feammox activity and perfluorooctanoic acid (PFOA) degradation by Acidimicrobium sp. Strain A6 using PAA-coated ferrihydrite as an electron acceptor, J. Hazard Mater. 459 (2023) 132039, https://doi.org/10.1016/j.jhazmat.2023.132039.

[11] S. Rahim Pouran, A.A. Abdul Raman, W.M.A. Wan Daud, Review on the application of modified iron oxides as heterogeneous catalysts in Fenton reactions, J. Clean. Prod. 64 (2014) 24–35, https://doi.org/10.1016/j.jclepro.2013.09.013.

[12] D.R. Schlesinger, C. McDermott, N.Q. Le, J.S. Ko, J.K. Johnson, P.A. Demirev, Z. Xia, Destruction of per/poly-fluorinated alkyl substances by magnetite nanoparticle-catalyzed UV-Fenton reaction, Environ. Sci.: Water Res. Technol. 8 (2022) 2732–2743, https://doi.org/10.1039/D2EW00058J.

[13] N. Pino, J. Quinchia, S. Gómez, J.F. Espinal, A. Montoya, D. López, Selective heterogeneous hydrodeoxygenation of acetophenone over monometallic and bimetallic Pt–Co catalyst, Phil. Trans. R. Soc. A. 379 (2021) 20200346, https://doi.org/10.1098/rsta.2020.0346.

[14] K.W. Cheah, M.J. Taylor, A. Osatiashtiani, S.K. Beaumont, D.J. Nowakowski, S. Yusup, A.V. Bridgwater, G. Kyriakou, Monometallic and bimetallic catalysts based on Pd, Cu and Ni for hydrogen transfer deoxygenation of a prototypical fatty acid to diesel range hydrocarbons, Catal. Today 355 (2020) 882–892, https://doi.org/10.1016/j.cattod.2019.03.017.

[15] M. Wang, Y. Liu, H. Shi, S. Li, S. Chen, Yielding hydroxyl radicals in the Fenton-like reaction induced by manganese (II) oxidation determines Cd mobilization upon soil aeration in paddy soil systems, Environ. Pollut. 292 (2022) 118311, https://doi.org/10.1016/j.envpol.2021.118311.

[16] B.K. Min, A.K. Santra, D.W. Goodman, Understanding silica-supported metal catalysts: Pd/silica as a case study, Catal. Today 85 (2003) 113–124, https://doi.org/10.1016/S0920-5861(03)00380-8.

[17] L. Wu, L. Shi, S. Zhou, J. Zhao, X. Miao, J. Guo, Direct growth of CoFe2 alloy strongly coupling and oxygen-vacancy-rich CoFe2O4 porous hollow nanofibers: an efficient electrocatalyst for oxygen evolution reaction, Energy Technol. 6 (2018) 2350–2357, https://doi.org/10.1002/ente.201800298.

[18] G. Bharath, N. Ponpandian, Hydroxyapatite nanoparticles on dendritic α-Fe $_2$ O $_3$ hierarchical architectures for a heterogeneous photocatalyst and adsorption of Pb(ii) ions from industrial wastewater, RSC Adv. 5 (2015) 84685–84693, https://doi.org/10.1039/C5RA15703J.

[19] Y. Fang, T. Zhang, Y. Wang, Y. Chen, Y. Liu, W. Wu, J. Zhu, The highly efficient cathode of framework structural Fe2O3/Mn2O3 in passive direct methanol fuel cells, Appl. Energy 259 (2020) 114154, https://doi.org/10.1016/j.apenergy.2019.114154.

[20] T. Bao, M.M. Damtie, K. Wu, X.L. Wei, Y. Zhang, J. Chen, C.X. Deng, J. Jin, Z.M. Yu, L. Wang, R.L. Frost, Rectorite-supported nano-Fe3O4 composite materials as catalyst for P-chlorophenol degradation: preparation, characterization, and mechanism, Appl. Clay Sci. 176 (2019) 66–77, https://doi.org/10.1016/j.clay.2019.04.020.

[21] P. Pal, A.K. Giri, S. Mahanty, A.B. Panda, Morphology-mediated tailoring of the performance of porous nanostructured Mn $_2$ O $_3$ as an anode material, CrystEngComm 16 (2014) 10560–10568, https://doi.org/10.1039/C4CE01334D.

[22] G. Yang, W. Yan, J. Wang, H. Yang, Fabrication and formation mechanism of Mn $_2$ O $_3$ hollow nanofibers by single-spinneret electrospinning, CrystEngComm 16 (2014) 6907–6913, https://doi.org/10.1039/C4CE00521J.

[23] Y. Ghaffari, S. Beak, J. Bae, S. Kim, M. Saifuddin, K.S. Kim, One-step fabrication of novel ultra porous Mn2O3-Fe2O3 @ SiO2: a versatile material for removal of organic pollutants from industrial wastewater at neutral pH, Separ. Purif. Technol. 285 (2022) 120259, https://doi.org/10.1016/j.seppur.2021.120259.

[24] S. Baek, Y. Ghaffari, J. Bae, Synthesis of Fe2O3/Mn2O3 nanocomposites and impregnated porous silicates for dye removal: insights into treatment mechanisms, Catalysts 12 (2022) 1045, https://doi.org/10.3390/catal12091045.

[25] T. Xu, H. Ji, Y. Gu, T. Tong, Y. Xia, L. Zhang, D. Zhao, Enhanced adsorption and photocatalytic degradation of perfluorooctanoic acid in water using iron (hydr) oxides/carbon sphere composite, Chem. Eng. J. 388 (2020) 124230, https://doi.org/10.1016/j.cej.2020.124230.

[26] A. Parashar, S. Sikarwar, R. Jain, Removal of pharmaceuticals from wastewater using magnetic iron oxide nanoparticles (IOPs), Int. J. Environ. Anal. Chem. 102 (2022) 117–133, https://doi.org/10.1080/03067319.2020.1716977.

[27] D. Talbot, J. Queiros Campos, B.L. Checa-Fernandez, J.A. Marins, C. Lomenech, C. Hurel, G.D. Godeau, M. Raboisson-Michel, G. Verger-Dubois, L. Obeid, P. Kuzhir, A. Bee, Adsorption of organic dyes on magnetic iron oxide nanoparticles. Part I: mechanisms and adsorption-induced nanoparticle agglomeration, ACS Omega 6 (2021) 19086–19098, https://doi.org/10.1021/acsomega.1c02401.

[28] MdA. Islam, I. Ali, S.M.A. Karim, MdS. Hossain Firoz, A.-N. Chowdhury, D.W. Morton, M.J. Angove, Removal of dye from polluted water using novel nano manganese oxide-based materials, J. Water Proc. Eng. 32 (2019) 100911, https://doi.org/10.1016/j.jwpe.2019.100911.
[29] Y. Liang, J. Ouyang, H. Wang, W. Wang, P. Chui, K. Sun, Synthesis and characterization of core–shell structured SiO2@YVO4:Yb3+,Er3+ microspheres, Appl. Surf. Sci. 258 (2012) 3689–3694, https://doi.org/10.1016/j.apsusc.2011.12.006.
[30] Š. Meškinis, A. Vasiliauskas, M. Andrulevičius, D. Peckus, S. Tamulevičius, K. Viskontas, Diamond like carbon films containing Si: structure and nonlinear optical properties, Materials 13 (2020) 1003, https://doi.org/10.3390/ma13041003.